Improving Fractional Vegetation Cover Estimation With Shadow Effects Using High Dynamic Range Images

Wei Chen, Zhe Wang, Xuepeng Zhang, Guangchao Li, Fengjiao Zhang, Lan Yang, Haijing Tian, and Gongqi Zhou

***Abstract*—Measured fractional vegetation cover (FVC) on the ground is very important for validation of the remote sensing products and algorithms. However, because of the influence of some factors such as the angle of illumination and vegetation density, the existence of vegetation shadows limits the accuracy of FVC estimation. This article proposes a deep learning method to reduce the FVC estimation error based on high dynamic range (HDR) images with vegetation shadows (HDR REC-DL method). The HDR REC-DL method can accurately extract FVC from HDR images with complex texture information on vegetation shadows. This method is based on the U-Net convolutional network structure for semantic segmentation of images containing vegetation shadows, and the segmentation results are less affected by vegetation types. Results from the HDR REC-DL method were highly similar to the vegetation segmentation results from visual interpretation. Values of the kappa coefficient, F1 score (F1), recall, and mean intersection over union of the HDR REC-DL method were 0.926, 0.942, 0.924, 0.916 for sunny weather and 0.903, 0.974, 0.983, and 0.895 for cloudy weather, respectively. Compared with the vegetation segmentation accuracy of the shadow-resistant algorithm, the HDR REC-DL method increases the kappa coefficient, F1, and mIOU by 21%, 16%, and 29% for sunny weather, and by 11.1%, 3.6%, and 10.3% for cloudy weather, respectively. The HDR REC-DL method provides a novel method for accurately estimating FVC from images containing vegetation shadows.**

***Index Terms*—Deep learning, fractional vegetation cover (FVC), high dynamic range (HDR) image, shaded vegetation.**

I. Introduction

VEGETATION is an important part of the terrestrial ecosystem and plays an important role in maintaining the balance of ecosystems, conserving water sources, and conserving water and soil [1]–[4]. Fractional vegetation cover (FVC) can be defined as the percentage of the vertical projection area of the vegetation above ground (including leaves, stems, and branches) within a statistical scope [5]. FVC is a key parameter that reflects the growth status of vegetation and plays a key role in carbon and water cycles and evaluation of the ecological environment [6]–[8]. Currently, FVC is mainly obtained by ground measurement method and remote sensing estimation method.

The remote sensing estimation method uses satellite images to estimate FVC on a global or regional scale. There are many remote sensing inversion methods for FVC, and the commonly used methods include empirical model method, physical model method, mixed pixels decomposition method, and machine learning method [9]–[14]. Some researchers use empirical models, regression models and relationship models based on vegetation index to estimate FVC [9], [15]. The physical model method is to establish a model about the physical relationship between vegetation spectral information and FVC by studying the interaction between light and vegetation [13], [14]. Due to the problem of mixed pixels in satellite imagery, the dimidiate pixel model is proposed to distinguish vegetation and background information [10]. Several studies estimate global FVC based on VIIRS surface reflectance data using machine learning methods, such as back propagation neural networks and general regression networks [12].Some studies use deep learning regression models to estimate FVC in savanna ecosystems [11].

Although the remote sensing estimation method can easily and quickly estimate the FVC over large areas, the ground measured FVC is very important to verify the accuracy of remote sensing algorithms and products. At present, FVC ground measurement methods mainly include visual estimation, sampling, and photography [16]–[19]. The visual estimation method and the sampling method have the characteristics of low efficiency and high cost, while the photographic method can obtain vertical observation images of vegetation more quickly, which greatly improves the efficiency and accuracy of ground measurements. For the method of estimating FVC based on digital images, some studies use red-green-blue (RGB), hue saturation value, International Commission on Illumination L∗a∗b (LAB) and other color spaces to segment vegetation [20]–[22]. Some studies use threshold methods based on vegetation indices to estimate FVC,

Manuscript received October 18, 2021; revised December 27, 2021 and January 23, 2022; accepted January 25, 2022. Date of publication February 4, 2022; date of current version February 16, 2022. This work was supported in part by the Beijing Natural Science Foundation under Grant 8192037, in part by the Key Research and Development Program of Guangxi under Grant AB18050014, in part by the National Natural Science Foundation of China under Grant 41701391 and Grant 41901301, and in part by Yue Qi Young Scholar Project, CUMTB. *(Corresponding author: Wei Chen.)*

Wei Chen, Zhe Wang, Xuepeng Zhang, Guangchao Li, Fengjiao Zhang, and Lan Yang are with the School of Geoscience and Surveying Engineering, China University of Mining and Technology, Beijing 100083, China (e-mail: chenw@cumtb.edu.cn; wangzhe_cumtb@163.com; 996588861@qq.com; lgc911201@163.com; jiao970924@126.com; ylannn2020@163.com).

Haijing Tian is with the Academy of Inventory and Planning, National Forestry and Grassland Administration, Beijing 100714, China (e-mail: tianhaijing278@163.com).

Gongqi Zhou is with the Beijing TerraQuanta Technology Company, Ltd., Beijing 100102, China (e-mail: zhou@terraqt.com).

Digital Object Identifier 10.1109/JSTARS.2022.3148282

such as the color index of vegetation extraction and excessive green index [23]–[26]. However, these methods generally have better effects on specific types of vegetation and are affected by the complexity of vegetation texture information. There are also some studies that use machine learning methods to estimate FVC, mainly via supervised and unsupervised classification methods to perform cluster analysis on training samples [27], [28].

With the development of deep learning algorithms, convolutional networks have become the preferred method for analyzing medical images [29]. Convolutional neural networks (CNNs) are deep feed-forward neural networks that show great potential in vegetation classification and segmentation in the agricultural field [30]–[32]. When the image has complex texture information, the segmentation effect of classic CNNs and machine learning methods will be greatly affected and are generally limited to small labeled datasets. However, the U-shaped neural network (U-Net) model overcomes these problems in image segmentation. The architecture of the U-Net model includes a contracting path for capturing context and a symmetrical expansive path for precise positioning [33]. Some studies use deep learning methods based on CNNs to segment tropical rainforest habitat images and have achieved good segmentation results [34].

However, due to the influence of factors such as the angle of sunlight, the density of vegetation, and the angle of the camera relative to the sun and vegetation, specular reflections and shadows are formed on vegetation. Due to the existence of shadows, it can be very difficult to segment vegetation from the background of the image [35], [36]. The presence of shadows will increase the error of vegetation classification, which will lead to missing and over-segmentation of the vegetation segmentation results in the shadow area, which will greatly affect the estimation accuracy of FVC [37], [38]. However, high dynamic range (HDR) images can solve the problems of natural lighting changes and large differences in image intensity. It is obtained by synthesizing the best details of the low dynamic range image corresponding to each exposure time, which can better show the characteristics of vegetation in shadow areas. [39] and [40]. Many studies have shown that under direct sunlight, the dynamic range of HDR image scenes is much larger than that of traditional non-HDR images, especially when the image scene contains shadows [41]. Some studies combine photos with different exposures into HDR images. For objects that show shadow areas, HDR images produce better results than single exposure images [42]. Some studies have proposed a ground shadow detection and removal algorithm based on the color space conversion of HDR images and multilevel thresholds to improve the performance of vegetation segmentation [41].

Therefore, to reduce the influence of shadows on FVC estimation, this research study proposes a deep learning method based on HDR images containing vegetation shadows to reduce FVC estimation errors (HDR REC-DL method). This method uses a U-shaped CNN, which has a jump-connected codec structure that can integrate features at different levels [33]. The vegetation shadow contained in the image has a fixed structure and contains substantial texture information. It is more suitable for segmentation of images containing vegetation shadows based on the deep learning method of U-shaped neural networks. The HDR image is created by merging three images with different exposures. Spanning a wide range of exposures will cause the shadows to become brighter [42]. It can better display the texture and detailed characteristics of the vegetation in the shadow and can improve the segmentation effect of the HDR REC-DL method on images containing vegetation shadows.

The rest of this article is organized as follows. The sample datasets and the processing flow of the HDR REC-DL method are described in Section II. Section III introduces the relevant experimental results of using the HDR REC-DL method and traditional threshold method to calculate FVC. Section IV discusses the advantages and limitations of the HDR REC-DL method. Finally, the experimental results of this article are summarized in Section V.

II. Data and Methods

A. Dataset Description

In this article, a Huawei Honor 10 smartphone was used to take the HDR and normally exposed photos with vegetation shadows. The vegetation images were obtained under various light and weather conditions within a few days in May, June, July, September, and November 2021. The shooting location was near the Huailai Remote Sensing Comprehensive Test Station in Donghuayuan Town, Huailai County, Hebei Province. The surface around the test station is rich in types, including farmland, waters, mountains, grasslands, and wetlands. The smartphone was installed on a tripod approximately 1 m above the ground, and Bluetooth was used to control the camera. HDR images and normal exposure images can be obtained by setting the phone camera to HDR mode and normal exposure mode, respectively. The focal length and International Standards Organization (ISO) of the camera were 4 mm and 50, respectively.

Labelme is an image labeling software with a graphical interface. Labelme software can label images in the form of polygons, rectangles, circles, polylines, line segments, and points [43]. It can be used for tasks such as target detection and image segmentation. For the image dataset containing vegetation shadows used in this article, Labelme software provided pixel-level annotations for two semantic classes, including background (soil, straw, stone, etc.) and foreground (vegetation in shaded areas, vegetation in illuminated areas). In this article, HDR and normally exposure vegetation images (121 groups) were taken under sunny and cloudy weather, 46 sets of data were selected as the test sets, and the remainder were the training (52 groups) and validation sets (23 groups). The 26 and 20 groups of data in the test sets were taken in sunny weather and cloudy weather, respectively. The HDR image, the normal exposure image, and the respective labels were cropped into square images with a size of 512×512. To expand the datasets, $*$ the sample images and labels were cropped with a step size of 256 to obtain 19965 subsample images and labels. Among them, there are 7590 test sets of subsamples and a total of 12 375 training and validation sets. The 12 375 subsamples were randomly divided into training

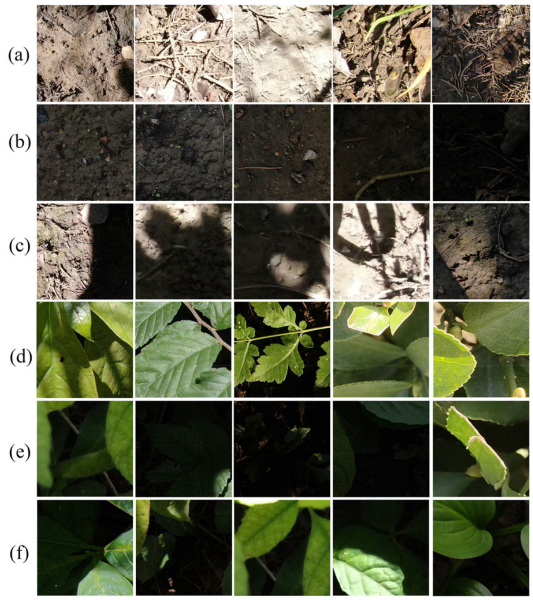

Fig. 1. Soil and vegetation types in the subsample dataset (size 512 × 512). (a)–(f) The types of ground objects represented are illuminated soil, shadow soil, illuminated and shadow mixed soil, illuminated vegetation, shaded vegetation, and illuminated and shadow mixed vegetation.

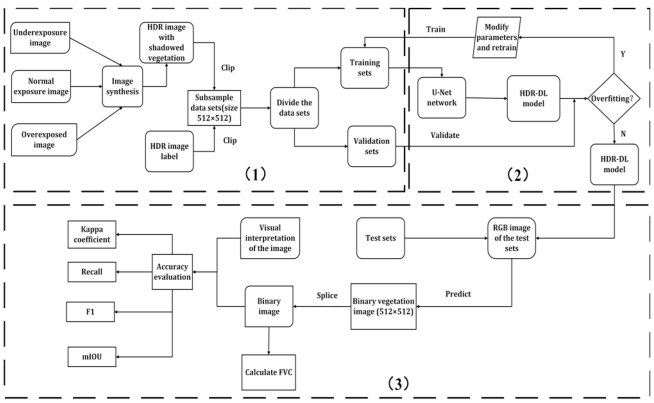

Fig. 2. Flow chart of the HDR REC-DL method segmenting HDR images containing vegetation shadows to calculate FVC.

sets and validation sets at a ratio of 7:3. Fig. 1 shows the main feature types selected from the 512 × 512 subsample datasets.

B. HDR REC-DL Method

According to Fig. 2, this flowchart is mainly divided into three parts. In the first part, HDR images are synthesized and datasets are created. First, through the HDR mode in the smartphone camera, the HDR image with vegetation shadows is taken. The vegetation is marked to obtain the label of the vegetation area in the image. The HDR images and labels are cropped into subsample datasets of 512 × 512, and the subsample datasets are divided into training sets, validation sets, and test sets. In the second part, the HDR-DL model is trained. The training sets are placed into the U-Net network to train the HDR-DL model, and the validation set data is used to determine whether the model is overfitting. In the third part, the HDR-DL model is

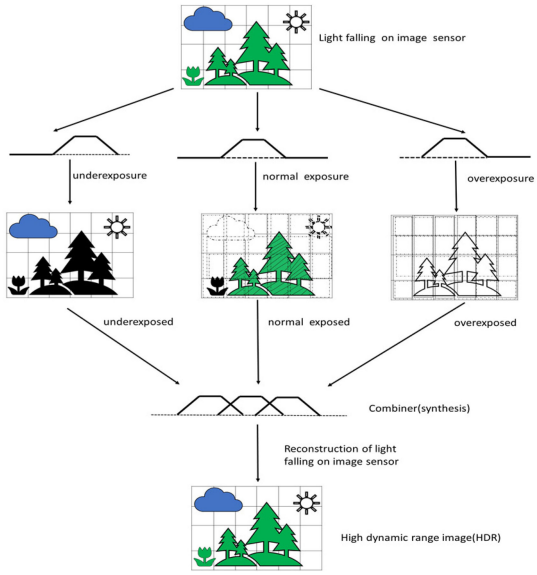

Fig. 3. Schematic diagram of composite HDR images.

used to segment the vegetation in the subsample test sets. The trained HDR-DL model is utilized to predict the HDR images in the subsample test sets to obtain binary vegetation images and calculate FVC. Then, the kappa coefficient, recall, F1 score (F1), and mean intersection over union (mIOU) are calculated to evaluate the accuracy of the HDR REC-DL method for FVC estimation of HDR images with vegetation shadows.

HDR imaging (HDRI) is a technology used to achieve a larger dynamic range of exposure than ordinary digital imaging technology [44]. The purpose of HDRI is to correctly represent the brightness in the real world from direct sunlight to the darkest shadow. In natural scenes, the dynamic brightness range refers to the ratio of the highest light intensity to the lowest light intensity [39]. The dynamic range of an image can be defined as the logarithmic ratio between the largest and smallest readable signal in a given scene [44]

$$\text{Dynamic Range}\,(\text{dB}) = 20 \times \log_{10} \frac{\text{Max Signal}}{\text{Min Signal}}. \quad (1)$$

At present, the commonly used method to obtain HDR images is to synthesize images based on multiple exposures [45]. The process of synthesizing HDR images is shown in Fig. 3. The HDR images are images with three exposure types: low exposure, normal exposure, and overexposure, and the best details of images with different exposure times are used to synthesize the HDR images [46]. The key to this method is exposure bracketing and merging. For nonlinear RGB images, the response curve must be calibrated first, and the nonlinear RGB image is converted into a linearized image [47]. The relationship between them is as follows:

$$I_{\text{non-linear}}(x, y) = f\left[I_{\text{linear}}(x, y)\right] \quad (2)$$

where $I_{\text{non-linear}}(x, y)$ is the pixel value of the nonlinear image; $I_{\text{linear}}(x, y)$ is the pixel value of the linear image; and f is the camera response function.

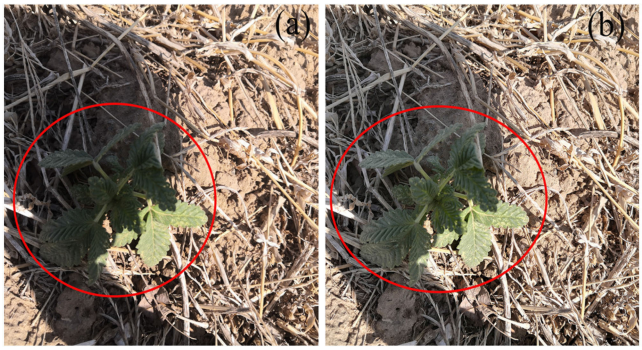

Fig. 4. Uncropped normal exposure image and HDR image. (a) Normal exposure image. (b) HDR image. The red circle indicates the difference in brightness between the vegetation shadows in the normal exposure image and the HDR image.

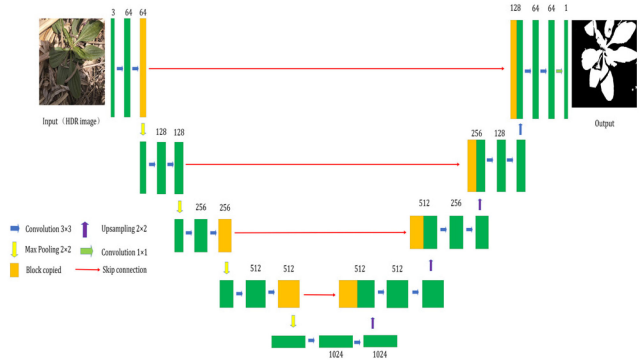

Fig. 5. U-Net architecture used to segment vegetation types that contain shadows. The number of channels is displayed above the rectangle.

The pixel value in the image can be changed by changing the exposure time. The pixel value of the linear image and the irradiance of the scene with different exposure times can be expressed as

$$I_{\text{linear}}(x,y) = \text{clip}\left(t_i L(x,y) + n\right) \tag{3}$$

where $L(x,y)$ is the irradiance of the scene; t_i is the exposure time of the *i*th image, i = 1, 2, 3 ($t_1 = 1/200\ s,\ t_2 = 1/640\ s,\ t_3 = 1/1250\ s$); and *n* is the noise.

For each pixel, the valid pixel value is found in the photo with different exposure times. A pixel value less than 0.05 is considered noise, and a pixel value greater than 0.95 is considered an overexposed area. The valid pixel value range is [0.05, 0.95]. The corresponding weight $w_i(x,y)$ of these pixel values is obtained, and the final pixel value of the position in the different exposure photos is generated by weighted fusion. The equation is as follows:

$$w_i(x,y) = \frac{I_i(x,y)}{t_i} \tag{4}$$

$$\text{out}(x,y) = \sum_{i=1}^{3} w_i(x,y)\, I_i(x,y) \tag{5}$$

where $w_i(x,y)$ is the weight, $I_i(x,y)$ is the valid pixel value of the *i*th image, and $out(x,y)$ is the fused HDR image.

Fig. 4(a) and (b) shows that the shadows in the normally exposed images are darker in color, and the texture features of the vegetation are not obvious. However, the shadow area of the HDR image becomes brighter and lighter in color, and the outline and texture of the vegetation in the shadow area displayed are clearer.

The HDR REC-DL method uses a U-Net CNN to train the model. It combines high-resolution features and upsampling layer output to provide pixel-level positioning. The U-Net structure has a large number of feature channels, which allows the network to propagate contextual information to higher resolution layers. In the U-shaped structure, the expansion path and the contraction path are symmetrical [33]. The deep learning model is implemented in the programming environment of PyTorch+python3.7. The U-Net network structure used in this article is shown in Fig. 5. The network is a semantic segmentation network composed of a fully convolutional network, a residual network and a feature pyramid network structure [48]. The cross-entropy loss function used is shown in

$$\text{cross}_{\text{entropy}} = -\sum_{x} \left(p_i(x) \log q_i(x)\right) \tag{6}$$

where $p_i(x)$ represents the label of the sample i, the positive class is 1, and the negative class is 0; $q_i(x)$ represents the probability that the sample i is predicted to be a positive class.

The multiplication operation in the commonly used cross-entropy loss function is improved to the addition operation, which will not change the monotonicity of the function and can greatly improve the operation speed. The Adam optimizer is used to backpropagate the loss function value [49]. It cannot only automatically adjust the learning rate to adapt to large-scale data operations but also has the advantages of high computational efficiency and small memory requirements, as shown in

$$W_{t+1} = W_t - \frac{\eta}{\sqrt{\hat{v}_t} + \varepsilon} * \hat{m}_t \tag{7}$$

where W_t is the weight value in t iterations; η is the momentum vector; m_t and v_t are the first-order and second-order momentum terms, respectively; $\hat{m}_t$ and $\hat{v}_t$ are the correction values; and ε is a very small number.

The loss value is calculated using the loss function, and the weight value in the model is adjusted through back propagation according to the loss value. The overfitting of the model is judged according to the accuracy of the segmentation results of the training set and the validation set. If the model is overfitting, then the learning rate, number of iterations, initial value, momentum coefficient and other parameters in the model can be modified to retrain the network. The HDR-DL model can be obtained after continuous parameter adjustment. This makes the accuracy indicators of the training sets and the validation sets converge. Through model prediction, the segmentation result of the image containing the vegetation shadows is obtained. After parameter modification, the final parameters of the HDR-DL model are 8 batches and 70 iterations, and the learning rate of the optimized function is 0.001.

C. SHAR-LABFVC Method

The threshold selection method is a simple and commonly used image segmentation technique that can divide the image into foreground and background [50], [51]. The classification of images containing vegetation shadows is a difficult problem in digital image processing. The existence of shadows will increase the error of vegetation and background classification. Some studies have proposed a shadow-resistant algorithm (SHAR-LABFVC method) based on the LABFVC algorithm [52], [53].

The SHAR-LABFVC method first converts the RGB color space into the hue saturation intensity (HSI) space and performs histogram equalization on the intensity components. The original intensity is replaced with the equalized intensity and reconvert the image to the RGB color space. After that, the RGB color space is converted to the LAB color space. The green vegetation and the background are fitted with the normal distribution function and the Gaussian distribution function of the $a*$ component, respectively, and then the threshold is calculated to classify the vegetation and the background. The fitting function of the distribution of green vegetation and background on the $a*$ component is shown in

$$F(x) = \frac{w_v}{x \cdot \sigma_v \sqrt{2\pi}} e^{\frac{-(lnx-\mu_v)^2}{2\sigma_v^2}} + \frac{w_b}{\sigma_b \sqrt{2\pi}} e^{\frac{-(x-\mu_b)^2}{2\sigma_b^2}} \tag{8}$$

where the dependent variable $F$is the frequency of green vegetation and background on the $a*$ component. μ_{v} and μ_{b} are the mean values of green vegetation and background, respectively; σ_v and σ_b are the standard deviations of green vegetation and background, respectively; and w_v and w_b are the weights of green vegetation and background, respectively.

The SHAR-LABFVC method can be divided into the SHAR-LABFVC empirical method, SHAR-LABFVC T1 method, and SHAR-LABFVC *T*2 method according to different selection thresholds. In the SHAR-LABFVC empirical method, the empirical threshold *T* is suggested to be -4, which could be changed according to difference conditions [52]. For the SHAR-LABFVC *T*1 method, the threshold *T*1 is calculated according to the principle of the minimum total commission error of vegetation and background, as shown in

$$AT^2 + BT + C = 0 \tag{9}$$

$$T_1 = \frac{-B \pm \sqrt{B^2 - 4AC}}{2A}. \tag{10}$$

In the SHAR-LABFVC *T*2 method, the *T*2 threshold is calculated based on the idea that the misclassification probabilities of vegetation and background are equal. A complementary error function is combined to determine the *T*2 threshold

$$\mathrm{erf}c(x) = 1 - \mathrm{erf}(x) = \frac{2}{\sqrt{\pi}} \int_x^{\infty} e^{-t^2} dt. \tag{11}$$

When the classification error of vegetation is equal to the classification error of the background, the optimal threshold *T*2 is as shown in

$$w_v \cdot \mathrm{erf}c\left(\frac{T_2 - \mu_v}{\sqrt{2}\sigma_v}\right) = w_b \cdot \mathrm{erf}c\left(\frac{T_2 - \mu_b}{\sqrt{2}\sigma_b}\right) \tag{12}$$

where $\mathrm{erf}c$ is the Gaussian error function.

In this article, the best vegetation segmentation results of the three thresholds of the SHAR-LABFVC method are used as the final results of the SHAR-LABFVC method.

TABLE I
CONFUSION MATRIX

Ground truth	Algorithm		
	Vegetation	Background	Total
Vegetation	TP	FN	N_{1+}
Background	FP	TN	N_{2+}
Total	N_{+1}	N_{+2}	N

N_{+i} is the sum of the number of pixels in the i-th column. N_{i+} is the sum of the number of pixels in the *i*th row. N is the total number of pixels.

D. Performance Evaluation

The segmentation results of the vegetation are compared with the results of visual interpretation to evaluate the segmentation effect. The confusion matrix (see Table I) is used to quantitatively evaluate the effect of vegetation segmentation on images containing vegetation shadows. This article uses the kappa coefficient, F1 score (F1), recall and mIOU to quantitatively analyze the results of the segmentation of images with vegetation shadows. Recall is a measure of coverage, which measures how many positive cases are classified as positive cases. F1 is the harmonic average of precision and recall. The mIOU value is an important indicator that measures the accuracy of image segmentation. This indicator can be interpreted as the average intersection ratio, and the intersection over union (IOU) value is calculated for each category. By combining these indicators, it is helpful to better evaluate the performance of vegetation segmentation. The calculation formulas for these indicators are as follows:

$$\kappa = \frac{\sum_i X_{ii} - \sum_i N_{i+} N_{+i}}{N^2 - \sum_i N_{i+} N_{+i}} \tag{13}$$

$$\mathrm{Recall} = \frac{\mathrm{TP}}{\mathrm{TP} + \mathrm{FN}} \tag{14}$$

$$F1 = \frac{2 \times \mathrm{Precision} \times \mathrm{Recall}}{\mathrm{Precision} + \mathrm{Recall}} \tag{15}$$

$$\mathrm{IOU} = \frac{\mathrm{TP}}{\mathrm{TP} + \mathrm{FP} + \mathrm{FN}} \tag{16}$$

where κ is the kappa coefficient; X_{ii} is the value of the diagonal of the confusion matrix; F1 is the F1 score; IOU is the intersection over union; true positive (TP): the ground truth is vegetation, and the prediction result is vegetation; false negative (FN): the ground truth is vegetation, and the prediction result is background; false positive (FP): the ground truth is background, and the prediction result is vegetation; true negative (TN): the ground truth is background, and the prediction result is background.

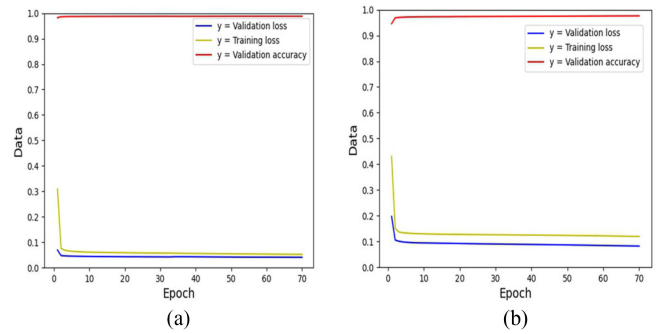

Fig. 6. Model evaluation of the HDR REC-DL method and NOR REC-DL method.

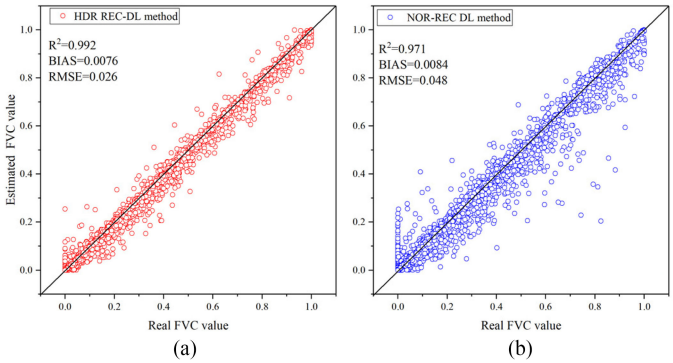

Fig. 7. Scatter plots of the FVC and true FVC estimated by the HDR REC-DL method and NOR REC-DL method (the subsample image type include purely illuminated soil and purely shaded soil).

III. Results

A. Evaluation of Segmentation Results of Subsamples by the REC-DL Method

A deep learning method based on normal exposure images (NOR) with vegetation shadows is proposed to reduce FVC estimation errors (NOR REC-DL method). The NOR REC-DL method and HDR REC-DL method are deep learning methods based on normal exposure images and HDR images, respectively. The difference between the two methods is mainly the different types of images processed. After 70 iterations, the accuracy of the model trained by the HDR REC-DL method on the validation sets is 0.987, and the loss on the validation sets and training sets is 0.053 and 0.041, respectively. Similarly, after 70 iterations, the accuracy of the model trained by the NOR REC-DL method on the validation sets is 0.976, the validation set loss is 0.083, and the training set loss is 0.120. Fig. 6 shows that as the number of iterations continues to increase, the validation set loss of the HDR REC-DL method and NOR REC-DL method gradually stabilizes.

For all types of test set subsample images in sunny weather, the FVC estimated by the HDR REC-DL method and the NOR REC-DL method are compared with the visually interpreted FVC true value, and the scatter plot is shown in Fig. 7. Fig. 7 shows that the correlation between the FVC calculated by the HDR REC-DL method and the visually interpreted FVC true value is stronger

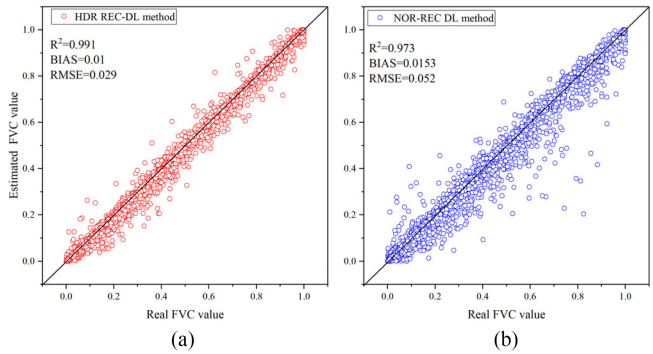

Fig. 8. Scatter plots of the FVC and true FVC estimated by the HDR REC-DL method and NOR REC-DL method (the subsample image type does not include purely illuminated soil and purely shaded soil).

than that of the NOR REC-DL method. The BIAS and RMSE of the HDR REC-DL method are 0.0076 and 0.026, respectively, which are lower than the NOR REC-DL method. In addition, the NOR REC-DL method misclassifies pure soil as vegetation in more images than the HDR REC-DL method. This means that when the soil pixels in a normally exposed image are dark, they will be classified as vegetation. For the 3093 test set subsample images that do not include purely illuminated soil and purely shaded soil, the scatter plots between the HDR REC-DL method, NOR REC-DL method and the visually interpreted FVC true value are shown in Fig. 8. For the subsample dataset that does not include purely light and purely shaded soil, the R^2, BIAS, and RMSE of the HDR REC-DL method are 0.991, 0.01, and 0.029, respectively. On the whole, the HDR REC-DL method is better than the NOR REC-DL method with regard to the FVC estimation results of the subsamples, and the results are closer to the visually interpreted true value.

The results of 5 sets of subsample experiments (A to E) are selected for display. According to Fig. 9, compared with the visual interpretation, the vegetation segmentation results in the shaded area using the NOR REC-DL method are partially missing. The NOR REC-DL method demonstrates inadequate vegetation segmentation results in the C and D experiments but is slightly more effective in the A and B experiments. This is because the vegetation shadows in images C2 and D2 are very dark, and the veins and textures of the vegetation leaves in images A2 and B2 are not obvious in the shadows. These factors will cause a lack of vegetation segmentation results in the NOR REC-DL method. In the E group experiment, the NOR REC-DL method exhibits a small amount of oversegmentation, which misclassifies the straw as vegetation. However, the HDR REC-DL method demonstrates the best effect on the segmentation of vegetation in the shadow area, and its segmentation results have high similarities with the results of visual interpretation. To better measure the classification accuracy of vegetation in subsample images containing vegetation shadows, four indicators, namely, the kappa coefficient, F1, recall and mIOU, are used to evaluate the classification accuracy. The four classification indices of the 4290 subsamples of the statistical test sets are given in Table II.

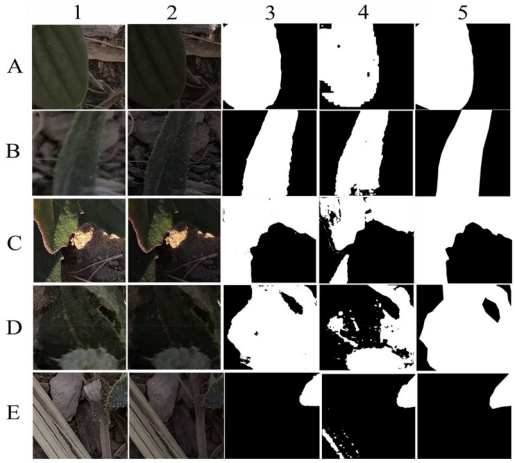

Fig. 9. Vegetation segmentation results of the HDR REC-DL method and the NOR REC-DL method on the subsample images with vegetation shadows. The images in columns (1) and (2) are the HDR image and normal exposure image, respectively. The images in columns (3)–(5) are the classification results from the HDR REC-DL method, NOR REC-DL method and visual interpretation, respectively. A to E represent the image and vegetation classification results of different experiments.

TABLE II
STATISTICS OF FOUR VEGETATION CLASSIFICATION INDICATORS FOR THE HDR REC-DL METHOD AND NOR REC-DL METHOD (4290 SUBSAMPLES)

	Kappa	F1	Recall	mIOU
Mean (HDR)	0.74	0.89	0.87	0.83
Median (HDR)	0.90	0.95	0.94	0.90
Std (HDR)	0.33	0.15	0.18	0.16
Mean (NOR)	0.66	0.82	0.79	0.76
Median (NOR)	0.79	0.89	0.89	0.81
Std (NOR)	0.32	0.20	0.24	0.15

For the subsample image data, overall, the vegetation segmentation effect of the HDR REC-DL method is better than that of the NOR REC-DL method. Compared with the NOR REC-DL method, the HDR REC-DL method exhibits the largest improvement with regard to the kappa coefficient, which are increased by approximately 13.3%. F1 value, recall, mIOU increased by 8.9%, 9%, and 8.7%, respectively.

B. Evaluation of FVC Estimation Results of the Entire Images

The HDR REC-DL method and the NOR REC-DL method can obtain the overall binary image of 26 groups (in sunny weather) and 20 groups (in cloudy weather) test sets by stitching the predicted subsample binarized images. We compare the FVC estimated by the HDR REC-DL method, NOR REC-DL method, SHAR-LABFVC method with the visually interpreted true value of FVC. Fig. 10(a) shows that the FVC estimation result of the HDR REC-DL method is closer to the true value than the NOR REC-DL method in sunny weather, and the FVC estimation deviation of the former is smaller than that of the latter. The correlation between the FVC estimation result of the HDR REC-DL method and the visually interpreted FVC is greater than that of the NOR REC-DL method in sunny weather. Fig. 10(c) illustrates that the difference between the FVC estimation results

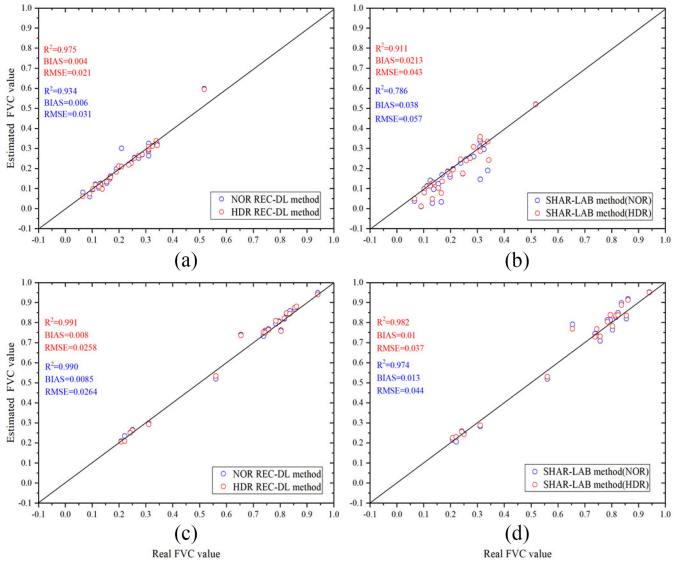

Fig. 10. Scatter plot of the FVC estimated by the HDR REC-DL method, NOR REC-DL method, SHAR-LABFVC method (NOR, HDR) (in sunny and cloudy weather). NOR represents that the processed image is normal exposure images, and HDR represents that the processed image is HDR images.

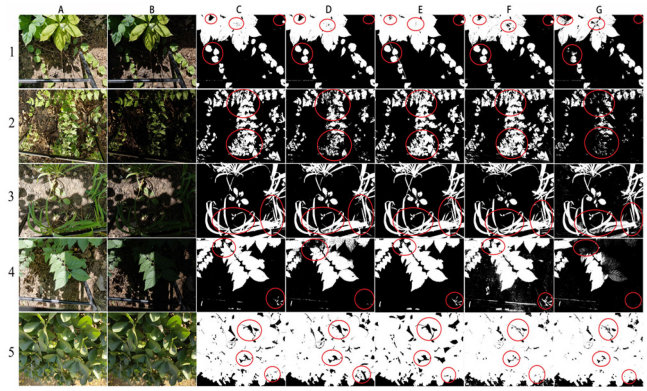

Fig. 11. Vegetation segmentation results from different methods in sunny weather. (a) HDR image. (b) Normal exposure image, (c) Classification result of the HDR REC-DL method. (d) NOR REC-DL method. (e) Visual interpretation. (f) SHAR-LABFVC method (HDR). (g) SHAR-LABFVC method (NOR).

of the HDR REC-DL method and the NOR REC-DL method is small in cloudy weather. According to Fig. 10(b) and (d), The BIAS and RMSE of the SHAR-LABFVC method (HDR) are lower than the SHAR-LABFVC method (NOR) in sunny and cloudy weather. In sunny and cloudy weather, the coefficient of determination of the four methods from high to low is the HDR REC-DL method, the NOR REC-DL method, SHAR-LABFVC method (HDR), SHAR-LABFVC method (NOR). On the whole, the HDR REC-DL method produces the most accurate FVC estimation than the other three methods.

Five sets of results are selected to show the visual effects of different methods on vegetation segmentation under sunny weather conditions. In the sequence numbers C to G, white represents the vegetation, and black represents the background. According to Fig. 11, the HDR REC-DL method has the best visual effect of vegetation segmentation in sunny weather, and

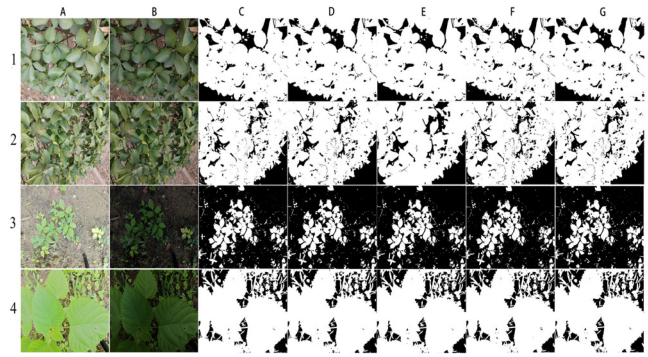

Fig. 12. Vegetation segmentation results of different methods in cloudy weather. (a) HDR image. (b) Normal exposure image. (c) Classification result of the HDR REC-DL method. (d) NOR REC-DL method. (e) Visual interpretation. (f) SHAR-LABFVC method (HDR). (g) SHAR-LABFVC method (NOR).

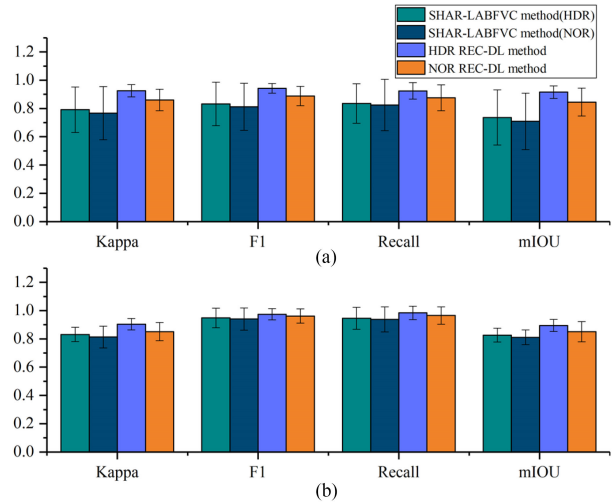

Fig. 13. Vegetation segmentation accuracy index of the SHAR-LABFVC method, the HDR REC-DL method, and the NOR REC-DL method. (a) Sunny weather. (b) Cloudy weather.

the SHAR-LABFVC method (NOR) is the worst. For the clustered vegetation in Fig. 11 (the fifth row), the SHAR-LABFVC method incorrectly divides the dry yellow and dead leaves into vegetation, and there is noise in the background of the segmentation result. For short canopy vegetation images with deep shadows, the SHAR-LABFVC method (NOR) and NOR REC-DL method will distinguish the part of the vegetation in the shadow area as the background. The wrong segmentation of the former is more serious than the latter. The SHAR-LABFVC method (NOR) has a poor segmentation effect for vegetation with obvious leaf veins in shallow shadow areas, and the segmentation results have more noise. In Fig. 11 (the third and fourth rows of images), the soil moisture types are moist soil and dry soil, respectively. Comprehensive analysis of the visual results of the vegetation segmentation of 26 sets of test images, the HDR REC-DL method, and the NOR REC-DL method is less affected by the type of soil moisture, and there is less noise in the vegetation segmentation results. However, the SHAR-LABFVC method is seriously affected by the type of soil moisture, and some vegetation segmentation results have more noise. For photos with vegetation shadows taken in sunny weather, the visual effects of vegetation segmentation from satisfactory to unsatisfactory are the HDR REC-DL method, NOR REC-DL method, SHAR-LABFVC method (HDR), and SHAR-LABFVC method (NOR).

According to the segmentation results of the clustered plants in cloudy weather in Fig. 12 (the first and second rows of images), it can be found that the vegetation segmentation results of the four methods have very little difference. This may be related to the absence of shadows in the image of clustered plants under cloudy conditions. For the short canopy vegetation in Fig. 12 (the third and fourth rows of images), the visual results of the four methods of vegetation segmentation have small differences. The soil moisture type in Fig. 12 (the third row of the image) is moist soil. The results of the SHAR-LABFVC method show that there are a small number of small noise points classified as vegetation, especially in the moist soil area on the right half of the image. However, the results of the HDR REC-DL method and the NOR REC-DL method have fewer noise points than the SHAR-LABFVC method. This means that the HDR REC-DL method and the NOR REC-DL method are less affected by the type of soil moisture in cloudy weather.

The average values of the four indicators of the vegetation segmentation results in the 26 groups (photographed in sunny weather) and 20 groups of photos (photographed in cloudy weather) are shown in Fig. 13. According to Fig. 13(a), the four indicators of the HDR REC-DL method are the highest in sunny weather, and those of the SHAR-LABFVC method (NOR) are the lowest. The kappa coefficient, F1, recall, and mIOU of the HDR REC-DL method are 0.926, 0.942, 0.924, and 0.916, respectively. For the HDR REC-DL method, these four indicators are increased by 7.6%, 6%, 5.6%, and 8.4% compared with the NOR REC-DL method. For the HDR REC-DL method, the kappa coefficient, F1, recall, and mIOU are increased by 21%, 16%, 12%, and 29%, respectively, compared with the SHAR-LABFVC method (NOR). As illustrated in Fig. 13(b), the average values of the kappa coefficient, F1, recall, and mIOU of the HDR REC-DL method in cloudy weather are 0.903, 0.974, 0.983, and 0.895, respectively. For these four indicators under cloudy conditions, the HDR REC-DL method is 6.1%, 1%, 1.9%, 5.2%, and 11.1%, 3.6%, 4.9%, 10.3% higher than the NOR REC-DL method and the SHAR-LABFVC method (NOR), respectively.

According to the comprehensive results of these four indicators, the accuracy of these methods for image segmentation with vegetation shadows ranges from satisfactory to unsatisfactory as follows.

the HDR REC-DL method, NOR REC-DL method, SHAR-LABFVC method (HDR), SHAR-LABFVC method (NOR).

IV. Discussion

A. Advantages of the HDR REC-DL Method

The novelty of this article is mainly to combine HDR images with U-Net CNN and propose an FVC inversion method combined with deep learning. HDR images can weaken the

strong light, highlight the information in the low-light area, and better display the vegetation information in the shadow area [42]. The U-Net CNN combines low-resolution information that provides the basis for vegetation identification and high-resolution information that provides the basis for accurate segmentation and positioning [33]. This method can effectively reduce the influence of shadows due to strong changes in natural light and direct sunlight. It can significantly improve the estimation accuracy of FVC.

The angle of sunlight, natural light changes and the occlusion of vegetation leaves will cause shadows in the captured vegetation images. These shadows present a tremendous challenge for accurately estimating FVC. The presence of shadows can lead to incorrect classification of vegetation in shadow areas [35]. The SHAR-LABFVC method is better for certain types of shaded vegetation. However, for images with complex scenes and different types of shaded vegetation, especially for elaborate texture information, the vegetation in the shaded area will be over segmented or missing [52]. However, the HDR REC-DL method does not use thresholds to segment shadow vegetation and is less affected by vegetation types. The U-Net CNN used can effectively analyze the texture information of vegetation leaves. Texture information can not only reveal the characteristics of vegetation, but also help segment vegetation with complex texture information [54]. By analyzing the context signals of multiple adjacent pixels, it is possible to better segment the vegetation in the shadow area with complex texture information [48].

In this article, the HDR REC-DL method improves the estimation accuracy of FVC compared with the NOR REC-DL method and SHAR-LABFVC method. In the verification of the FVC of different images, this method has demonstrated a lower RMSE and bias, and the estimated FVC is closest to the true value. The vegetation segmentation results of the HDR REC-DL method are very similar to visually interpreted images, which improves the performance of images segmentation of vegetation with shadows under natural lighting conditions in the wild.

B. Limitations and Future Perspectives

The HDR REC-DL method studied clustered and short canopy vegetation, but did not study the segmentation effect of coniferous vegetation. This article is based on ground images and did not test the segmentation effect of this method on the unmanned aerial vehicle (UAV) scale. This article did not consider the influence of the change of the solar angle on the segmentation accuracy of the HDR REC-DL method.

In the future, the effect of this method in estimating FVC in coniferous vegetation and UAV images can be further evaluated. The changes of the solar angle will affect the area, position, and depth of shadows in the vegetation image. We will further study the impact of changes in the solar angle on the HDR REC-DL method in future research. Besides, the canopy cover can be further used to estimate leaf area index (LAI). However, the presence of shadows in digital images with a sky background can affect the accuracy of canopy cover estimation. The HDR images can better suppress strong light and highlight weak light. Thus, the HDR REC-DL method may be of great use for improving the accuracy of calculating LAI.

V. Conclusion

The HDR REC-DL method proposed in this article combines the advantages of HDR images and U-shaped CNNs, which can efficiently and accurately estimate the FVC of images with vegetation shadows. The HDR REC-DL method improves the segmentation performance of vegetation in shadow areas under natural light conditions. The FVC results of subsample images (including shadow vegetation) estimated by the HDR REC-DL method and NOR REC-DL method are compared. The HDR REC-DL method is better than the NOR REC-DL method with respect to the vegetation segmentation effect of subsamples containing vegetation shadows. This shows that the deep learning method based on HDR images improves the FVC estimation accuracy of the images with vegetation shadows in the subsamples. For the spliced subsample images, the four indicators of the kappa coefficient, F1, recall, and mIOU are comprehensively analyzed. The order of segmentation effect of the vegetation from satisfactory to unsatisfactory is the HDR REC-DL method, NOR REC-DL method, SHAR-LABFVC method (HDR), and SHAR-LABFVC method (NOR). The HDR REC-DL method is suitable for segmenting images of vegetation shadows with complex scenes and texture information. The vegetation segmentation effect is less affected by vegetation types. The HDR REC-DL method provides a novel method for measuring FVC as ground verification data.

References

[1] D. D. Kong *et al.*, "Seasonal vegetation response to climate change in the northern hemisphere (1982-2013)," *Glob. Planet. Change*, vol. 148, pp. 1–8, Jan. 2017.

[2] A. A. Gitelson *et al.*, "Novel algorithms for remote estimation of vegetation fraction," *Remote Sens. Environ.*, vol. 80, no. 1, pp. 76–87, Apr. 2002.

[3] X. Wen, X. Deng, and F. Zhang, "Scale effects of vegetation restoration on soil and water conservation in a semi-arid region in China: Resources conservation and sustainable for management," *Resour. Conserv. Recycling*, vol. 151, Dec. 2019, Art. no. 104474.

[4] C. J. Kucharik *et al.*, "Testing the performance of a dynamic global ecosystem model: Water balance, carbon balance, and vegetation structure," *Glob. Biogeochem. Cycles*, vol. 14, no. 3, pp. 795–825, Sep. 2000.

[5] K. Wittich and O. Hansing, "Area-averaged vegetative cover fraction estimated from satellite data," *Int. J. Biometeorol.*, vol. 38, no. 4, pp. 209–215, 1995.

[6] H. H. Feng, B. Zou, and J. H. Luo, "Coverage-dependent amplifiers of vegetation change on global water cycle dynamics," *J. Hydrol.*, vol. 550, pp. 220–229, Jul. 2017.

[7] M. Jung *et al.*, "Exploiting synergies of global land cover products for carbon cycle modeling," *Remote Sens. Environ.*, vol. 101, no. 4, pp. 534–553, Apr. 2006.

[8] Y. Wang and M. Li, "Annually urban fractional vegetation cover dynamic mapping in Hefei, China (1999-2018)," *Remote Sens.*, vol. 13, no. 11, Jun, 2021, Art. no. 2126.

[9] J. F. Xiao and A. Moody, "A comparison of methods for estimating fractional green vegetation cover within a desert-to-upland transition zone in Central New Mexico, USA," *Remote Sens. Environ.*, vol. 98, no. 2-3, pp. 237–250, Oct. 2005.

[10] J. L. Case, F. J. LaFontaine, J. R. Bell, G. J. Jedlovec, S. V. Kumar, and C. D. Peters-Lidard, "A real-time MODIS vegetation product for land surface and numerical weather prediction models," *IEEE Trans. Geosci. Remote Sens.*, vol. 52, no. 3, pp. 1772–1786, Mar. 2014.

[11] W. Li *et al.*, "Deep-learning based high-resolution mapping shows woody vegetation densification in Greater Maasai Mara ecosystem," *Remote Sens. Environ.*, vol. 247, Sep. 2020, Art. no. 111953.
[12] D. Y. Liu *et al.*, "Global fractional vegetation cover estimation algorithm for VIIRS reflectance data based on machine learning methods," *Remote Sens.*, vol. 10, no. 10, Oct. 2018, Art. no. 1648.
[13] W. Verhoef, "Light scattering by leaf layers with application to canopy reflectance modeling: The SAIL model," *Remote Sens. Environ.*, vol. 16, no. 2, pp. 125–141, Jan. 1984.
[14] P. Scarth and S. Phinn, "Determining forest structural attributes using an inverted geometric-optical model in mixed eucalypt forests, Southeast Queensland, Australia," *Remote Sens. Environ.*, vol. 71, no. 2, pp. 141–157, Feb. 2000.
[15] J. P. Guerschman *et al.*, "Estimating fractional cover of photosynthetic vegetation, non-photosynthetic vegetation and bare soil in the Australian tropical Savanna region upscaling the EO-1 hyperion and MODIS sensors," *Remote Sens. Environ.*, vol. 113, no. 5, pp. 928–945, May 2009.
[16] X. B. Li *et al.*, "Improvement, comparison, and application of field measurement methods for grassland vegetation fractional coverage," *J. Integrative Plant Biol.*, vol. 47, no. 9, pp. 1074–1083, Sep. 2005.
[17] M. O. Smith *et al.*, "Vegetation in deserts: I. A regional measure of abundance from multispectral images," *Remote Sens. Environ.*, vol. 31, no. 1, pp. 1–26, 1990.
[18] B. C. Rundquist, "The influence of canopy green vegetation fraction on spectral measurements over native tallgrass prairie," *Remote Sens. Environ.*, vol. 81, no. 1, pp. 129–135, Jul. 2002.
[19] D. T. Booth *et al.*, "The accuracy of ground-cover measurements," *Rangeland Ecol. Manage.*, vol. 59, no. 2, pp. 179–188, Mar. 2006.
[20] Y. Liu *et al.*, "A novel method for extracting green fractional vegetation cover from digital images," *J. Vegetation Sci.*, vol. 23, no. 3, pp. 406–418, Jun. 2012.
[21] B. Panneton and M. Brouillard, "Colour representation methods for segmentation of vegetation in photographs," *Biosyst. Eng.*, vol. 102, no. 4, pp. 365–378, Apr. 2009.
[22] I. Philipp and T. Rath, "Improving plant discrimination in image processing by use of different colour space transformations," *Comput. Electron. Agriculture*, vol. 35, no. 1, pp. 1–15, Jul. 2002.
[23] T. Kataoka, T. Kaneko, H. Okamoto, and S. Hata, "Crop growth estimation system using machine vision," in *Proc. IEEE/ASME Int. Conf. Adv. Intell. Mechatronics*, 2003, pp. 1079–1083.
[24] C. Gee *et al.*, "Crop/weed discrimination in perspective agronomic images," *Comput. Electron. Agriculture*, vol. 60, no. 1, pp. 49–59, Jan. 2008.
[25] X. P. Burgos-Artizzu *et al.*, "Real-time image processing for crop/weed discrimination in maize fields," *Comput. Electron. Agriculture*, vol. 75, no. 2, pp. 337–346, Feb. 2011.
[26] G. E. Meyer and J. C. Neto, "Verification of color vegetation indices for automated crop imaging applications," *Comput. Electron. Agriculture*, vol. 63, no. 2, pp. 282–293, Oct. 2008.
[27] L. F. Tian and D. C. Slaughter, "Environmentally adaptive segmentation algorithm for outdoor image segmentation," *Comput. Electron. Agriculture*, vol. 21, no. 3, pp. 153–168, 1998.
[28] J. I. Corcoles *et al.*, "Estimation of leaf area index in onion (Allium cepa L.) using an unmanned aerial vehicle," *Biosyst. Eng.*, vol. 115, no. 1, pp. 31–42, May 2013.
[29] G. Litjens *et al.*, "A survey on deep learning in medical image analysis," *Med. Image Anal.*, vol. 42, pp. 60–88, Dec. 2017.
[30] A. Krizhevsky, I. Sutskever, and G. E. Hinton, "ImageNet classification with deep convolutional neural networks," *Commun. ACM*, vol. 60, no. 6, pp. 84–90, Jun. 2017.
[31] A. Kamilaris and F. X. Prenafeta-Boldu, "Deep learning in agriculture: A survey," *Comput. Electron. Agriculture*, vol. 147, pp. 70–90, Apr. 2018.
[32] U. Kalin *et al.*, "Defoliation estimation of forest trees from ground-level images," *Remote Sens. Environ.*, vol. 223, pp. 143–153, Mar. 2019.
[33] O. Ronneberger, P. Fischer, and T. Brox, "U-Net: Convolutional networks for biomedical image segmentation," in *Proc. Med. Image Comput. Comput.-Assist. Interv.*, 2015, pp. 234–241.
[34] J. F. Abrams *et al.*, "Habitat-Net: Segmentation of habitat images using deep learning," *Ecol. Informat*, vol. 51, pp. 121–128, May 2019.
[35] G. D. Finlayson *et al.*, "On the removal of shadows from images," *IEEE Trans. Pattern Anal. Mach. Intell.*, vol. 28, no. 1, pp. 59–68, Jan. 2006.
[36] H. Y. Jeon, L. F. Tian, and H. Zhu, "Robust crop and weed segmentation under uncontrolled outdoor illumination," *Sensors*, vol. 11, no. 6, pp. 6270–6283, Jun. 2011.
[37] W. Guo, U. K. Rage, and S. Ninomiya, "Illumination invariant segmentation of vegetation for time series wheat images based on decision tree model," *Comput. Electron. Agriculture*, vol. 96, pp. 58–66, Aug, 2013.
[38] A. T. Nieuwenhuizen *et al.*, "Colour based detection of volunteer potatoes as weeds in sugar beet fields using machine vision," *Precis. Agriculture*, vol. 8, no. 6, pp. 267–278, Dec. 2007.
[39] D. J. Graham, "Visual perception: Lightness in a high-dynamic-range world," *Curr. Biol.*, vol. 21, no. 22, pp. R914–R916, Nov. 2011.
[40] S. Mann *et al.*, "Realtime HDR (high dynamic range) video for eyetap wearable computers, FPGA-based seeing AIDS, and glasseyes (eyeTaps)," in *Proc. 25th IEEE Can. Conf. Elect. Comput. Eng.*, 2012, pp. 1–6.
[41] H. K. Suh, J. W. Hofstee, and E. J. van Henten, "Improved vegetation segmentation with ground shadow removal using an HDR camera," *Precis. Agriculture*, vol. 19, no. 2, pp. 218–237, Apr. 2018.
[42] S. E. Cox and D. T. Booth, "Shadow attenuation with high dynamic range images," *Environ. Monit. Assessment*, vol. 158, no. 1-4, pp. 231–241, Nov. 2009.
[43] A. Torralba, B. C. Russell, and J. Yuen, "LabelMe: Online image annotation and applications," *Proc. IEEE*, vol. 98, no. 8, pp. 1467–1484, Aug. 2010.
[44] C. Bloch, *The HDRI Handbook 2.0: High Dynamic Range Imaging For Photographers and CG Artists*. San Rafael, CA, USA: Rocky Nook, 2013.
[45] M. A. Robertson, S. Borman, and R. L. Stevenson, "Estimation-theoretic approach to dynamic range enhancement using multiple exposures," *J. Electron. Imag.*, vol. 12, no. 2, pp. 219–228, 2003.
[46] P. E. Debevec and J. Malik, "Recovering high dynamic range radiance maps from photographs," in *Proc. 24th Annu. Conf. Comput. Graph. Interactive Techn.*, 1997, pp. 369–378.
[47] S. Mann and R. Picard, "On being 'undigital' with digital cameras: Extending dynamic range by combining differently exposed pictures," in *Proc. IS&T 48th Annu. Conf. Soc. Imag. Sci. Technol. Annu. Conf.*, 1995, pp. 442–448.
[48] T. Kattenborn, J. Eichel, and F. E. Fassnacht, "Convolutional neural networks enable efficient, accurate and fine-grained segmentation of plant species and communities from high-resolution UAV imagery," *Sci. Rep.*, vol. 10, no. 1, 2019, Art. no. 17656.
[49] D. Kingma, and J. Ba, "Adam: A Method for Stochastic Optimization," *Int. Conf. Learn. Representat.*, Dec. 2014.
[50] Z. Wang, J. Xiong, Y. Yang, and H. Li, "A flexible and robust threshold selection method," *IEEE Trans. Circuits Syst. Video Technol.*, vol. 28, no. 9, pp. 2220–2232, Sep. 2018.
[51] B. Karasulu and S. Korukoglu, "A simulated annealing-based optimal threshold determining method in edge-based segmentation of grayscale images," *Appl. Soft Comput.*, vol. 11, no. 2, pp. 2246–2259, Mar. 2011.
[52] W. Song *et al.*, "Extracting the green fractional vegetation cover from digital images using a shadow-resistant algorithm (SHAR-LABFVC)," *Remote Sens.*, vol. 7, no. 8, pp. 10425–10443, 2015.
[53] X. Mu, Y. Liu, H. Wang, and G. Yan, "A novel method for extracting green fractional vegetation cover fromdigital images," *J. Vegetation Sci.*, vol. 23, no. 3, pp. 406–418, 2012.
[54] F. H. Wagner *et al.*, "Using the U-net convolutional network to map forest types and disturbance in the atlantic rainforest with very high resolution images," *Remote Sens. Ecol. Conserv.*, vol. 5, no. 4, pp. 360–375, Dec. 2019.

Wei Chen received the B.S. degree in geographical information system from Beijing Normal University, Beijing, China, in 2008 and Ph.D. degree in photogrammetry and remote sensing from Peking University, Beijing, China, in 2013.

He is currently an Associate Professor with the College of Geoscience and Surveying Engineering, China University of Mining & Technology, Beijing, China. His major research interests include remote sensing retrieval and remote sensing applications.

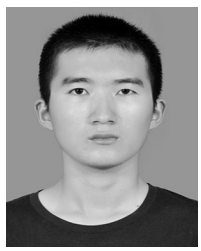

Zhe Wang is currently working toward the master's degree with the College of Geoscience and Surveying Engineering, China University of Mining and Technology, Beijing, China.

His major research interests include remote sensing of the ecological environment, computer vision, and deep learning.

Xuepeng Zhang is currently working toward the master's degree with the College of Geoscience and Surveying Engineering, China University of Mining and Technology, Beijing, China.

His current research interests include ecological value assessment and surface temperature inversion.

Guangchao Li is currently working toward the Ph.D. degree with the College of Geoscience and Surveying Engineering, China University of Mining and Technology, Beijing, China.

His current research interests include atmospheric aerosols, and ecological environment monitoring and evaluation.

Fengjiao Zhang is currently working toward the master's degree with the College of Geoscience and Surveying Engineering, China University of Mining and Technology, Beijing, China.

Her current research interests include satellite remote sensing radiometric calibration, land surface processes, and urban climate, and air quality.

Lan Yang is currently working toward the master's degree with the College of Geoscience and Surveying Engineering, China University of Mining and Technology, Beijing, China.

Her current research interests include polarization remote sensing, extraction of vegetables under shadow conditions, and application of deep learning in remote sensing.

Haijing Tian received the Ph.D. degree in cartography and geographic information systems from the Institute of Remote Sensing and Digital Earth, Chinese Academy of Sciences, Beijing, China, in 2017.

She is currently a Senior Engineer working with National Forestry Administration, Beijing, China.

Gongqi Zhou received the Ph.D degree in cartography and geographic information systems from Beijing Normal University, Beijing, China, in 2016.

He is the Lead basic Tech Scientist with TerraQuanta, Beijing, China. His research interests include remote sensing information extraction, computer vision, and machine learning.